

REPORT DOCUMENTATION PAGE			Form Approved OMB No. 0704-0188		
Public reporting burden for this collection of information is estimated to average 1 hour per response, including the time for reviewing instructions, searching data sources, gathering and maintaining the data needed, and completing and reviewing the collection of information. Send comments regarding this burden estimate or any other aspect of this collection of information, including suggestions for reducing this burden to Washington Headquarters Service, Directorate for Information Operations and Reports, 1215 Jefferson Davis Highway, Suite 1204, Arlington, VA 22202-4302, and to the Office of Management and Budget, Paperwork Reduction Project (0704-0188) Washington, DC 20503.					
PLEASE DO NOT RETURN YOUR FORM TO THE ABOVE ADDRESS.					
1. REPORT DATE (DD-MM-YYYY) 25-09-2002		2. REPORT TYPE Final Technical Report		3. DATES COVERED (From - To) 01 June 1998 - 30 June 2001	
4. TITLE AND SUBTITLE Development of A Nitric Oxide Monitor For Early Detection of Pathogenic Exposure (Final Technical Report)			5a. CONTRACT NUMBER		
			5b. GRANT NUMBER N65236-98-1-5415		
			5c. PROGRAM ELEMENT NUMBER DARPA Order No.: J484/00		
			5d. PROJECT NUMBER Program Code: P9310		
			5e. TASK NUMBER		
			5f. WORK UNIT NUMBER		
6. AUTHORS ESRG SRD					
7. PERFORMING ORGANIZATION NAME(S) AND ADDRESS(ES) UNIVERSITY OF MAINE OFFICE OF RESEARCH AND SPONSORED PROGRAMS 5717 CORBETT HALL ORONO, ME 04469-5717			8. PERFORMING ORGANIZATION REPORT NUMBER FINAL		
9. SPONSORING/MONITORING AGENCY NAME(S) AND ADDRESS(ES) SPACE AND NAVAL WARFARE SYSTEMS COMMAND (SPAWAR) SYSTEMS CENTER CHARLESTON P.O. BOX 190022 NORTH CHARLESTON, SC 29419-9022			10. SPONSOR/MONITOR'S ACRONYM(S) DARPA		
			11. SPONSORING/MONITORING AGENCY REPORT NUMBER		
12. DISTRIBUTION AVAILABILITY STATEMENT Approved for Public Release					
13. SUPPLEMENTARY NOTES			20021009 016		
14. ABSTRACT This project focused on three main topics: (i) determination of whether the nitric oxide (NO) level in exhaled human breath is a reliable diagnostic of respiratory distress, and in particular whether or not NO measurements can be used as a triage tool to identify human exposure to bio-warfare agents, (ii) research and engineering development of a small contact prototype NO breath monitor based on semiconducting metal oxide (SMO) thin film technology, and (iii) analysis of other breath components to identify additional potential biomarkers of disease using high resolution mass spectrometry. The work was performed by the Environmental Sensor Research Group (ESRG) which involves researchers from the University (UM), engineering staff from Sensor Research & Development (SRD) Corporation, and medical staff at Maine Medical Center (MMC).					
15. SUBJECT TERMS Nitric oxide breath sensor					
16. SECURITY CLASSIFICATION OF:			17. LIMITATION OF ABSTRACT UU	18. NUMBER OF PAGES 22	19a. NAME OF RESPONSIBLE PERSON Robert J. Lad
a. REPORT U	b. ABSTRACT U	c. THIS PAGE U			19b. TELEPHONE NUMBER (Include area code) 207-581-2257

FINAL REPORT

“DEVELOPMENT OF A NITRIC OXIDE MONITOR FOR EARLY DETECTION OF PATHOGENIC EXPOSURE”

Grant # N65236-98-1-5415

funded by

**Defense Advanced Research Projects Agency (DARPA)
Defense Sciences Office (DSO) - Advanced Diagnostics (AD)**

Project Period: June 1, 1998 – June 30, 2001

Grantee: University of Maine
Laboratory for Surface Science & Technology
5764 Sawyer Research Center, Orono, ME 04468-5764

Subcontractors: Sensor Research & Development Corporation
5 Godfrey Drive, Orono, ME 04473

Maine Medical Center
22 Bramhall Street, Portland, ME 04102

Table of Contents:

1. Executive Summary.....	1
2. Clinical Testing of NO Levels in Emergency Room Patients	2
3. Studies of NO Levels in a School Child Population	4
4. Optimization of Tungsten Oxide Thin Films for NO Detection	6
5. Prototype NO Chemiresistive Sensor System for Breath Sampling	9
6. Mass Spectral Measurements of Other Biomarkers in Human Breath	13
7. Research Publications and Presentations	20

1. Executive Summary

This project focused on three main topics: (i) determination of whether the nitric oxide (NO) level in exhaled human breath is a reliable diagnostic of respiratory distress, and in particular whether or not NO measurements can be used as a triage tool to identify human exposure to bio-warfare agents, (ii) research and engineering development of a small compact prototype NO breath monitor based on semiconducting metal oxide (SMO) thin film technology, and (iii) analysis of other breath components to identify additional potential biomarkers of disease using high resolution mass spectrometry. The work was performed by the Environmental Sensor Research Group (ESRG) which involves researchers from the University of Maine (UM), engineering staff from Sensor Research & Development (SRD) Corporation, and medical staff at Maine Medical Center (MMC).

Clinical data acquired from human subjects using a Sievers® laboratory-based chemiluminescence NO monitor led to several important conclusions. We found that exhaled NO levels were higher in emergency room patients with an infectious etiology indicating that NO is an important diagnostic of pathology. In addition, our data showed that smokers have lower exhaled NO values compared to non-smokers. The inherent variability of baseline values from individual to individual is problematic for using a single measurement as a meaningful diagnostic. However, exhaled NO values measured from a school child population revealed that NO levels appear to increase above baseline prior to usual infection symptoms, suggesting that the exhaled NO level is an important health diagnostic for both military and non-military use.

Small prototype nitric oxide sensors based on semiconducting metal-oxide (SMO) thin film technology were fabricated and characterized. A variety of SMO films were investigated including ruthenium oxide (RuO_2) and tungsten oxide (WO_3) thin films doped with either metal or metal-oxide catalyst species. Our results indicated that there is a negligible response towards NO for a wide variety of SMOs, but that the sensor responses towards NO_2 are very sensitive. These results lead to the development of a nitric oxide monitor that functions by first filtering out NO_2 and other interferents in breath. Then, the NO in the breath stream is oxidized to NO_2 , using one of several possible oxidizing agents, and then passed to the SMO thin film sensor for quantitative detection. Sensor performance studies of this prototype detection system demonstrated sensitivities to NO in breath samples in the 0-100 parts per billion range, which is well suited for real time medical monitoring. This nitric oxide monitor also showed relative insensitivity towards CO and CO_2 interferents.

Fourier transform ion cyclotron resonance (FT-ICR) mass spectrometry was used to analyze the specific components in human exhaled breath (HEB) other than NO. We identified the major components in HEB from "healthy" subjects including isoprene, acetone, pentane, ketones, and many other species. To achieve this, the design and construction of an improved ion source for qualitative and quantitative analysis of HEB and other complex sample matrices was carried out in collaboration with IonSpec (Irvine, CA). We successfully developed and constructed the instrumentation and software to identify each of the different components in HEB, including Mass Identification Smart Tool (MIST) software for unambiguous identification of unknown analytes. Several analytes were identified as potential biomarkers of pathology to assess human health status.

2. Clinical Testing of NO Levels in Emergency Room Patients

Over the past ten years, it has been identified that NO plays a critical role in diseases such as asthma, sepsis, hypertension and renal failure. NO is freely diffusable across membranes, is highly reactive, and is an important messenger which spontaneously decays after transmitting a signal. Production of NO is a common inflammatory pathway for bacteria, fungi, viruses, and parasites. The enzyme "nitric oxide synthase" is expressed in neuronal and endothelial cells and is also induced in macrophages where it has high enzymatic activity. In a rat LPS injection model (*Liu. Crit. Care Med.* 25, 512, 1997) it was reported that there is an upregulation of iNOS about 30 min after injection, that increases and plateaus in 4 to 8 hours and decreases by 24 hours. It is also known that NO originates in many tissues in the airway passage and in the vascular system. Furthermore, the literature has shown that in a rabbit-lung model (*AJRCCM* 157, 498 1998),

increases in expired NO parallel the increase in vascular levels, hence showing that the exhaled [NO] correlates with the serum [NO] levels.

As a follow-on to this data in the literature, we evaluated the use of exhaled NO as a diagnostic for respiratory distress using a group of emergency department patients at MMC who randomly came into the emergency room with sprained ankles, lacerations, various infections, etc. These patients had the stress and anxiety certainly like that people would have in a bioagent exposure scenario where they would be coming into the emergency rooms. The measurements were carried out using a commercial Sievers® model 280 chemiluminescence monitor. This is a large lab-based instrument that has become the current standard in the US medical community for NO analysis, but it requires two electrical outlets, weighs >80 pounds, and costs ~ \$30K. We used this instrument for the clinical NO measurements while the prototype compact NO monitor was being developed and evaluated.

A large amount of NO is produced in the nasal passages and therefore a restricted breath protocol was used where breath sampling is done using a large enough flow so as to close the velum and sample the NO from deep in the lungs. Figure 1 shows an example of exhaled NO data from a 32 year old WF emergency department cohort with an upper respiratory infection. When the patient blows at constant pressure for about 30 seconds, the NO signal comes to a steady state value which is the recorded [NO] value. This data is upon diagnosis of an infection and antibiotics were started immediately. After day 4 and day 10, the levels were back to baseline.

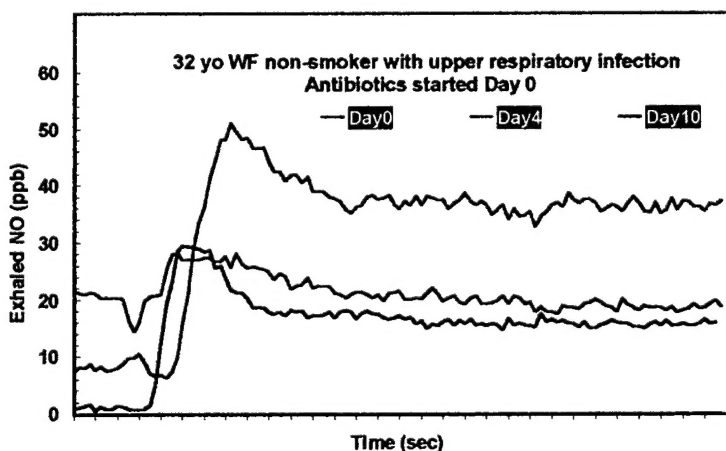


FIGURE 1 - Exhaled NO concentration versus time for an emergency room patient with an upper respiratory infection measured under constant breath flow.

Figure 2 shows data from the emergency department study: 20 patients without infections and 20 patients with either viral or bacterial infections. The healthy subjects have a baseline level in the 10 to 20 ppb range, but there are a few outliers. The mean value is 18.1 but a more meaningful number for such a small sample size is the median value of 13.9. For those cohorts with infections, both the mean and median values are significantly larger. A statistical t-test for this small sample data yields that the difference is meaningful within a 96 or 97% confidence level.

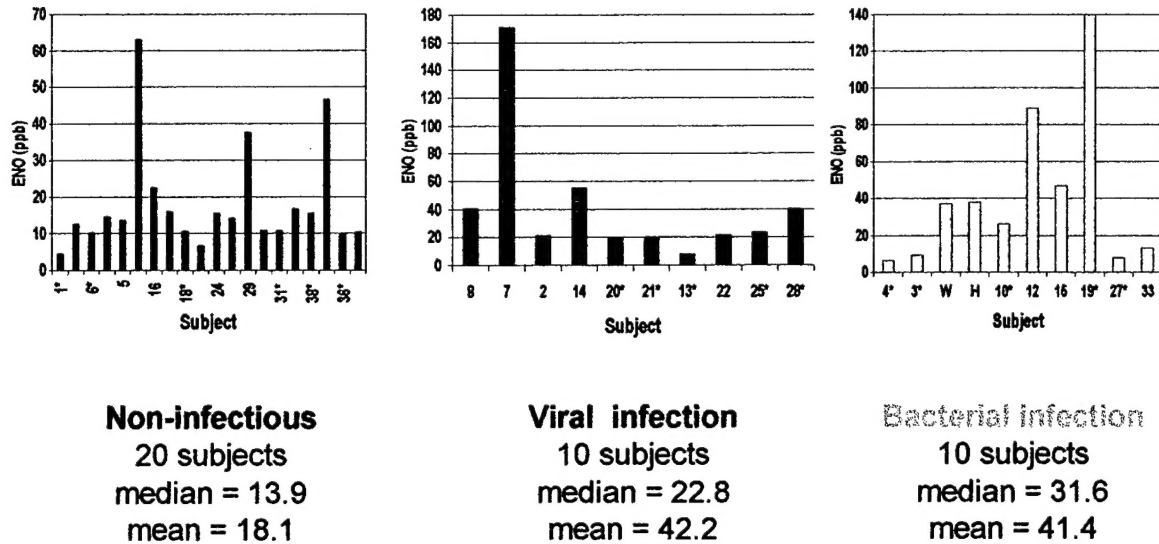


FIGURE 2 - Exhaled NO levels measured different emergency room patient populations. Note that the y-axis range differs for each graph. Smokers are denoted by *.

An important result that came out of our study is that smokers have a consistently lower exhaled NO level compared to nonsmokers as shown in Figure 3. This is true whether they are infectious or healthy. Those denoted with an * in Figure 2 are smokers. These results indicate that smokers potentially would show a false negative in a [NO] screening. The average [NO] values for the emergency room patients is summarized in Figure 4.

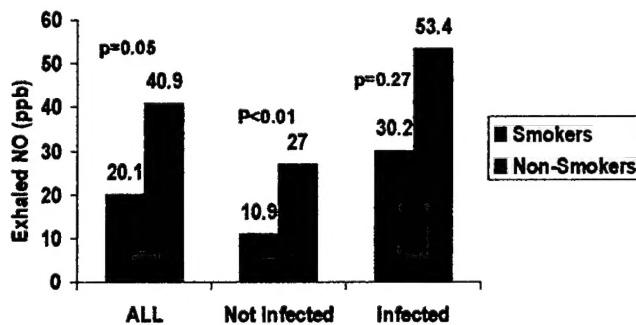


FIGURE 3 - Comparison of NO levels in smokers versus non-smokers.

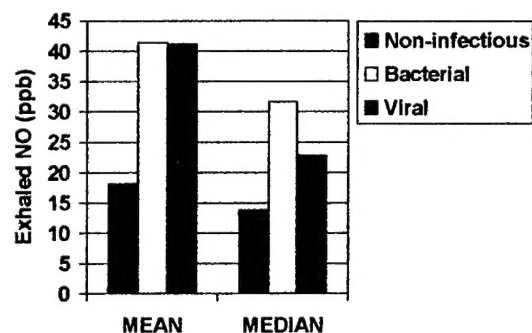


FIGURE 4 - Summary of average NO levels measured from healthy and infectious subjects in the emergency room study.

3. Studies of NO Levels in a School Child Population

The second population used for NO breath measurements was a group of 5th grade school children in the Cape Elizabeth Middle School. This sample set avoids complications such as smoking and alcohol use that are present in adult populations. We were looking for evidence for elevated NO levels as a very early indicator of respiratory distress, and this requires baseline data prior to getting sick. We accomplished this by doing a science project in the school classroom in which the students came in every day and blew into the Sievers® chemiluminescence monitor to generate

baseline [NO] data. This was carried out during January and February which are peak months for influenza in Maine. The students plotted the daily results and were truly excited about being participants in the experiment. We measured NO levels from 28 children and two examples are shown in Figure 5. The NO level is plotted versus health status as self reported by the students. Despite being a qualitative study with no clinical confirmation, these data clearly show that the NO levels are elevated prior to getting sick.

Monitor baseline and compare to values preceding illness symptom onset

▲ = no symptoms; ▲ = symptoms (cough, sore throat ...); ▲ = absent due to sickness

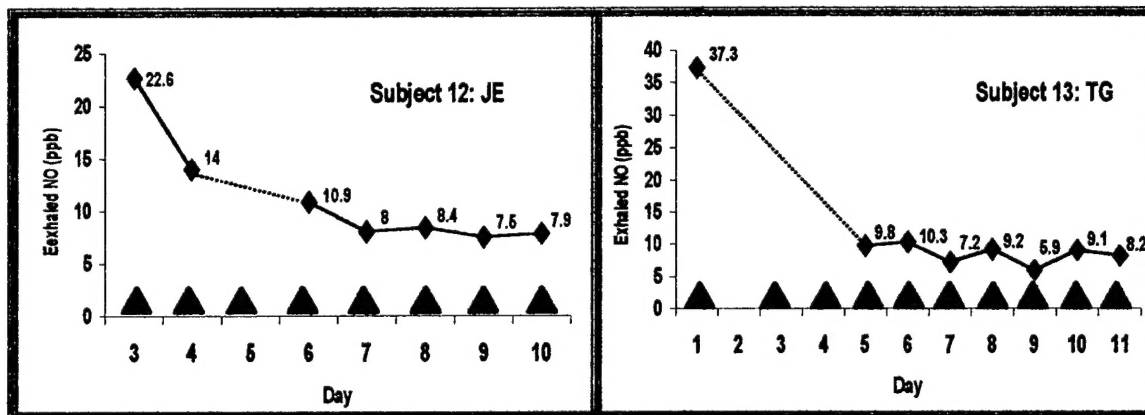


FIGURE 5 – Examples of NO levels from two school children showing that the elevated NO level occurs early in the infection as determined by qualitative self-reported symptoms.

The summary data shown in Figure 6 shows a clear indication that NO levels are larger in symptomatic subjects, and our child study seems to indicate that the NO is an early marker. However, using [NO] as a reliable diagnostic requires an established baseline level for a given subject prior to the infection. NO screening for pathogen exposure using a single measurement will not be a definitive test but potentially is very valuable in sorting the masses and determining who will need more immediate medical attention in a biowarfare scenerio. These studies demonstrated potential usefulness of expired NO as a clinical marker, but they also illustrate the need for more statistical data and correlation with additional clinical patient diagnostics. Furthermore, they motivate the need to fully analyze components of human breath and determine if other biomarkers are present in human breath that can be used in concert with the [NO] measurements.

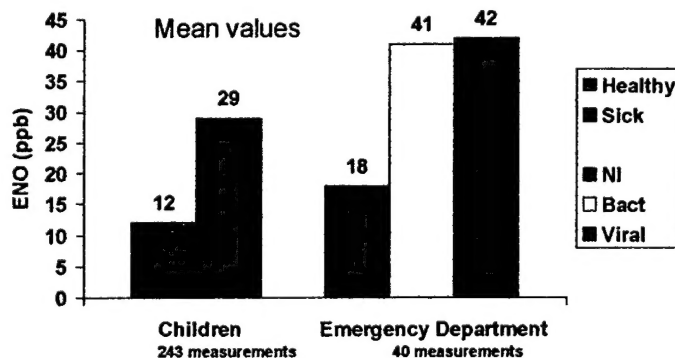


FIGURE 6 – Summary of clinical [NO] data measured from the school child and emergency room populations.

4. Optimization of Tungsten Oxide Thin Films for NO Detection

The need for a small compact NO monitor in the medical community which can conveniently and more affordably monitor the exhaled NO concentration led us to develop a SMO thin film based detection system. Applications of an NO breath analyzer require sensitivity in the range from several ppb to 1 ppm with selectivity against NO₂, CO, CO₂, and a range of hydrocarbons in the presence of relative humidity levels of approximately 100%. Therefore, a practical system must have sensitivity to NO, but also discriminate against perhaps a hundred common organic compounds present in breath. Although a large number of studies have been published related to the use of semiconducting metal oxide films for the detection of NO_x, relatively few make a clear distinction between the response toward NO and NO₂. Because NO can react very rapidly with oxygen and photoassisted reactions are well known, some care is required to deliver nitric oxide, while maintaining the concentration of the higher oxides below detection limits of the sensor. For this purpose, we utilized the Seivers® chemiluminescence monitor equipped with a converter for NO₂, so that the concentrations of both NO and NO₂ could be determined at an accuracy of 1 ppb prior to delivery to our prototype SMO sensors.

Sensor devices were fabricated by magnetron sputter deposition of a range of ultra-thin metal oxides on quartz, alumina and sapphire substrates. The semiconducting metal oxides investigated included RuO₂, RuO₂ modified with WO₃, SnO₂, Cu₂O, Ag₂O, Bi₂O₃, WO₃, and WO₃ modified with Pt, Ru or RuO₂. Nominal oxide thicknesses, as determined from a quartz crystal oscillator, ranged from 100 to 1000 Å and nominal thicknesses of the catalytic metal additives were varied from 5 to 50 Å. The best results were obtained by RF magnetron sputtering of WO₃ onto r-cut sapphire substrates grown under conditions leading to epitaxially oriented (polycrystalline) films.

The sensor platform upon which the oxide films were deposited consisted of platinum interdigitated electrodes on the top and a photolithographically patterned platinum RTD and serpentine heater on the back as shown in Figure 7. Sensors were operated typically at 250 °C to achieve rapid reaction kinetics and resistance was measured in the constant voltage mode. Using the known film thickness and geometry (6 parallel thin film resistors each of 500 Å thickness, 2.03 mm width, 0.254 mm length), the data was converted to conductivity.

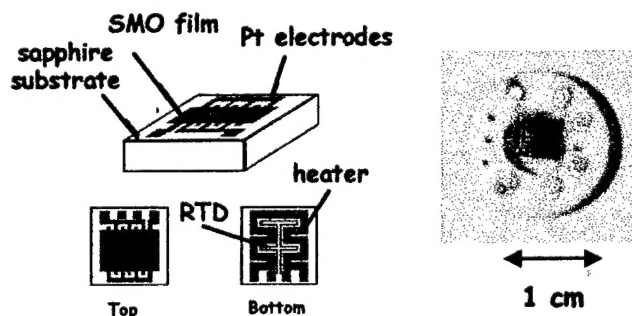


FIGURE 7 – SMO thin film on a chemiresistive sensor platform with integrated heater element. The sensor element is wire bonded into a TO-8 package.

Typical results for the negligible change in conductance of a WO_3 sensor element when exposed to NO in the range of 0-60 ppb is shown in Figure 8A. By contrast, exposure to NO_2 with a constant NO concentration shows a linear dependence over the range 0-30 ppb, as shown in Figure 8B.

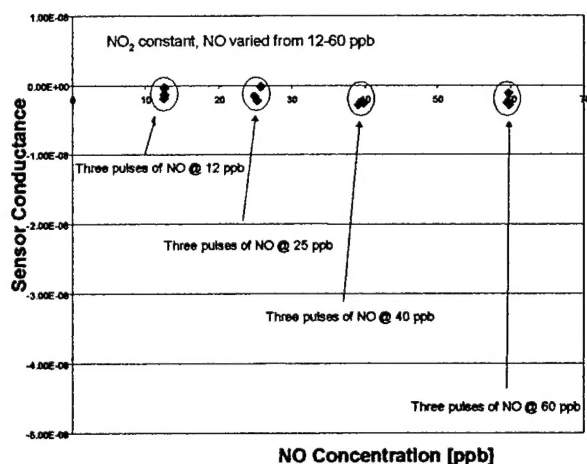


FIGURE 8A – SMO sensor response versus NO concentration at fixed NO_2 concentration.

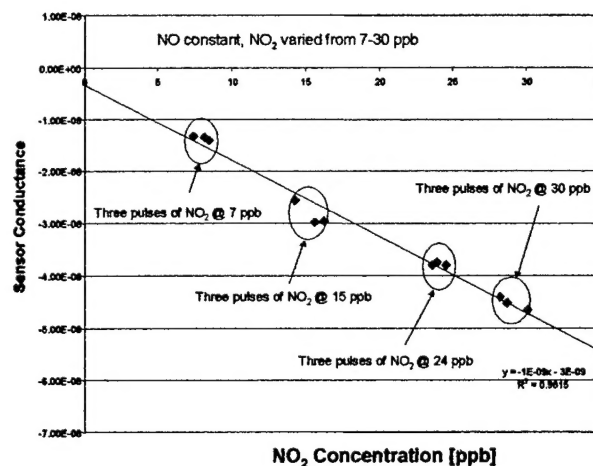


FIGURE 8B – SMO sensor response versus NO_2 concentration at fixed NO concentration.

The decrease in conductance when exposed to NO_2 is consistent with the oxidizing nature of the gas. Although evidence that NO can react with oxide surfaces in reducing environments when the oxide is highly reduced, the ambient air conditions in this case are unfavorable for reaction with NO. Using infrared spectrometry, we found negligible interaction between NO and a WO_3 surface. Even at temperatures as low as 150 K, physisorption of NO was not observed until the partial pressure was raised to around 1 torr, where condensation occurred. Conductivity measurements during exposure to NO at pressures up to 1 torr also showed no evidence for reaction with NO under vacuum conditions. The gas phase was monitored with a quadrupole mass spectrometer in the range up to 10^{-6} torr, and the infrared spectrum for pressures above 1 torr. Conversion of NO to NO_2 and N_2O_3 was observed only after several minutes at higher pressures (> 10 torr). Thus, even with relatively heavily reduced WO_3 surfaces, no evidence for adsorption or reaction of NO was found.

The sensitive and selective detection of NO_2 species is linear over the concentrations needed for the exhaled breath measurements. This result motivated the use of a NO_2 filter and NO oxidation catalyst to deliver NO_2 species arising from the NO in the breath sample to the SMO sensing element for quantification. A number of measurements were made to determine the sensitivity or cross-sensitivity with NO_2 to potential interferences. The concentration of CO_2 in exhaled breath can reach several percent. Figure 9A compares the sensor response to pulses of air containing 12% CO_2 , 50 ppb NO_2 , and mixtures of 12% CO_2 and 50 ppb NO_2 . Although the silicalite filter described below is expected to remove CO_2 species, oxidation products from the catalysts could potentially yield CO or CO_2 . However, the evidence from these results indicates that CO_2 does not interfere, either directly or together with NO_2 .

The variation in oxygen partial pressure also contributes to changes in conductivity through changes in the vacancy concentration. Therefore, the reaction rate of NO_2 with surface oxygen

vacancies could decrease with increasing oxygen pressure through a decrease in the surface vacancy concentration. A change in the oxygen concentration from 20% to 46% causes a relative change in conductivity of about 20% at 250 °C. The results shown in Figure 9B indicate that, although a change in oxygen concentration from 20% to 35% produces a measurable change in conductivity, the response to NO₂ is not significantly different.

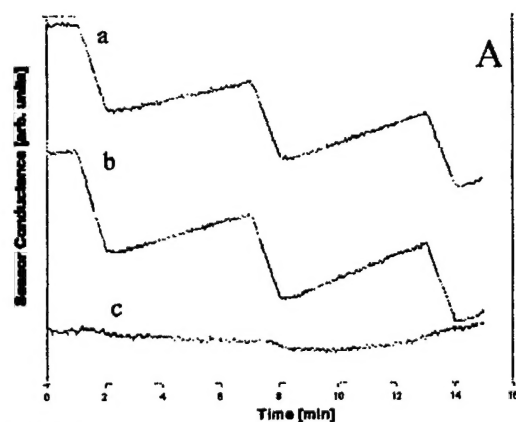


FIGURE 9A – Sensor response to three one minute pulses containing a) 50ppb NO₂ in air, b) 50ppb NO₂ and 12% CO₂ in air, and c) 12% CO₂ in air. Curves offset for clarity in both graphs.

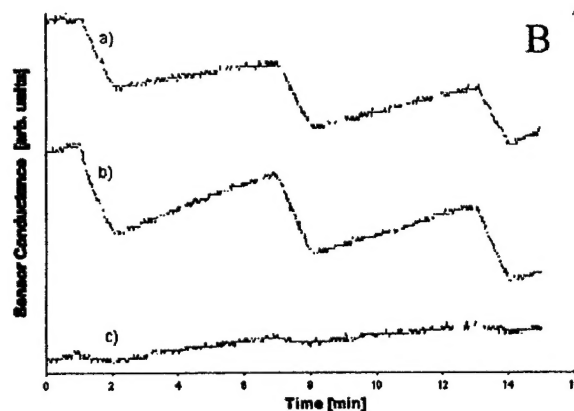


FIGURE 9B – Sensor response to three one minute pulses containing a) 50ppb NO₂ in air (20% O₂), b) 50ppb NO₂ and 35% O₂ in air, and c) 35% O₂ in air.

The response to a range of interferences is summarized in Table I. Sensor responses for each gas are simply categorized as causing a large (+++), moderate (++) or small increase (+), or a variable (+/-) response for concentrations within the range indicated. The concentration of each compound in human breath, based upon the work of Krotoszynski, et al. (*J. Chromatog. Sci.* **15**, 239, 1977) is shown for comparison. Note that all interferences tested result in an increase in conductivity, while response to NO₂ yields a decrease in conductivity. Thus, most organic interferences would produce a response which cancels that of NO₂, leading to an underestimate of the original NO concentration.

Potential Interferent	Range tested (Background air)	Sensor Response	Anticipated levels in breath*
Acetone	< 200 ppb	+	< 100 ppb
Isoprene	< 200 ppb	+++	< 100 ppb
Acetonitrile	< 200 ppb	+	< 100 ppb
p- Tolualdehyde	< 200 ppb	++	< 5ppb
2,4-Dimethylhexane	< 200 ppb	+/-	< 5ppb
Toluene	< 200 ppb	+	< 5ppb
Ethanol	< 200 ppb	+/-	< 5ppb
Acetaldehyde	< 200 ppb	+	< 5ppb
2,2,4-Trimethyl-1-Pentanol	< 200 ppb	++	< 5ppb
n-Pentane	< 200 ppb	+/-	< 5ppb
Methane	< 40 ppm	+/-	
Hydrogen	< 30 ppm	+/-	
Ammonia	< 15 ppm	+/-	
CO ₂	3-12%	+/-	
O ₂	16-35%	+/-	

TABLE I: Potential interferent components in breath with relative magnitude of sensor response and anticipated levels in breath.

The largest response of the compounds listed is due to isoprene, which is also one of the most prevalent compounds in exhaled breath. Figure 10 shows the response to varying concentrations of isoprene. The change in conductivity is reproducible and, at comparable concentrations, is sufficiently large to mask the response to nitric oxide. These results show that the quantitative removal of isoprene, and other organic constituents in breath, is clearly critical to practical operation of the NO monitor.

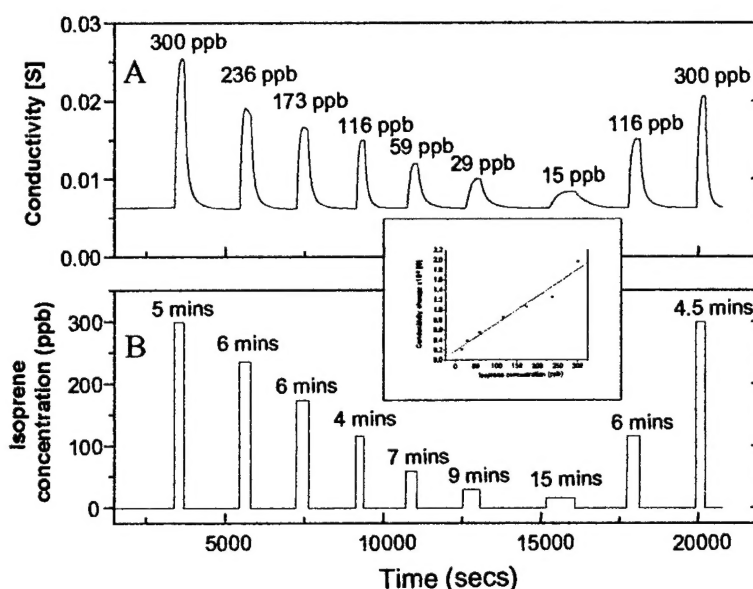


FIGURE 10 – Sensor response to varying concentrations of isoprene. The concentration given in A results from the gas pulse duration in B. The inset shows the conductivity change vs. isoprene concentration.

5. Prototype NO Chemiresistive Sensor System for Breath Sampling

The prototype NO monitoring system was constructed as shown in Figure 11. Breath samples in Tedlar bags and filtered air from a purification system (a Zero Contamination Filter, E. H. Lynn Industries, Inc., Romeoville, IL) were connected to a two way valve, allowing rapid switching between the two gas streams. The calibration gas (5 ppm NO in N₂) was added through a mass flow controller to the gas stream. A selective, semi-permeable membrane based upon a copolymer of tetrafluoroethylene and perfluoro-3,6-dioxo-4methyl-7-octene-sulfonic acid (Nafion, Perma Pure, Inc.) was used to equilibrate the humidity level to ambient conditions. A molecular sieve filter (Silicalite, PQ Corp., Valley Forge, PA) was provided to remove hydrocarbons and NO₂ from the gas stream, while allowing the nitric oxide to pass through. Oxidation of the nitric oxide was necessary prior to exposing the sensor to the gas stream. The total flow rate was controlled by a mass flow controller, typically placed at the end of the system, just prior to a low vacuum pump. Sensor temperature and resistance were controlled using custom designed circuitry developed around a Labview-based system. Concentrations of NO and NO₂ were determined simultaneously with the WO₃ sensor using the Sievers® chemiluminescence monitor equipped with a NO₂ to NO converter.

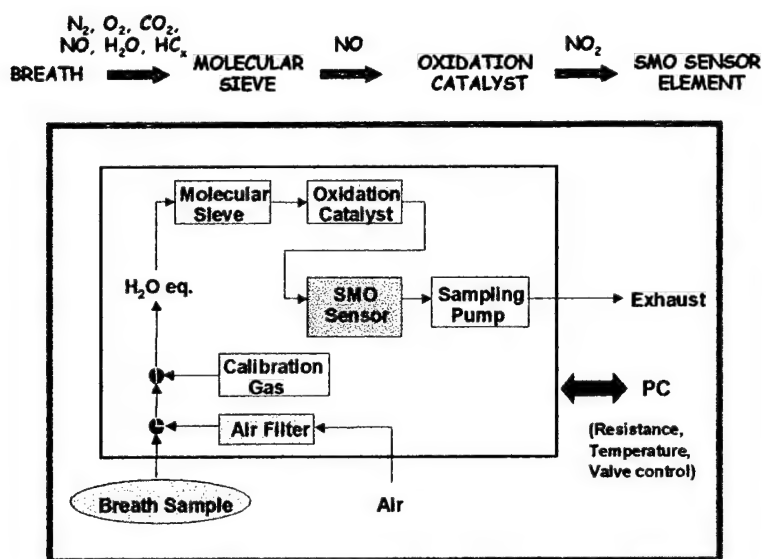


FIGURE 11 – Schematic diagram of the prototype NO monitor system.

The efficiency with which isoprene is removed from the gas stream by a silicalite filter is demonstrated in Figure 12. The filter in the prototype setup contained about 1 g of silicalite in a 1/4" OD by 4" long stainless steel tube. At concentrations as high as 200 ppb, the absorption of isoprene by the filter still reduced the sensor response to an acceptably small level. This data, taken with a humidity level of 15%, demonstrates the viability of the concept. Concern that water vapor might decrease the efficiency of the silicalite filter was investigated with GC/MS measurements. We found that isoprene (8.85 ppm in N_2) was reduced to levels of 10-20 ppb, both under dry conditions and in the presence of 100% relative humidity. The level of detection achieved with the GC/MS is indicated by the lowest detectable concentration of isoprene in standard solutions in hexane. Detection of 10 pg isoprene with a signal to noise level of 10 suggests a detection limit of 2 pg at a S/N of 2, which corresponds to a gas phase concentration of 2 ppb (w/w) in air. The removal of isoprene in the prototype system to levels below 20 ppb is consistent with the magnitude of sensor response shown in Figure 12.

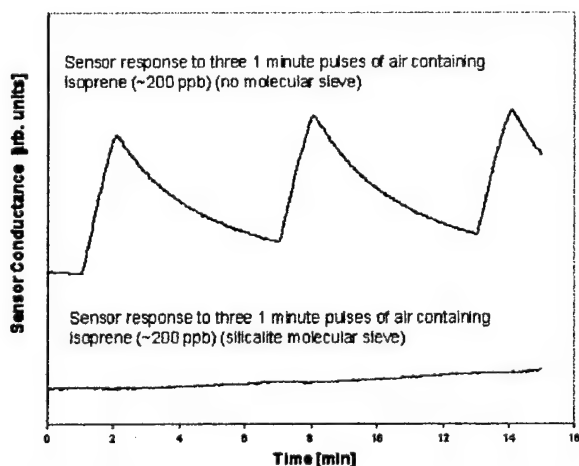


FIGURE 12 – Effectiveness of silicalite molecular sieve filter in removing isoprene.

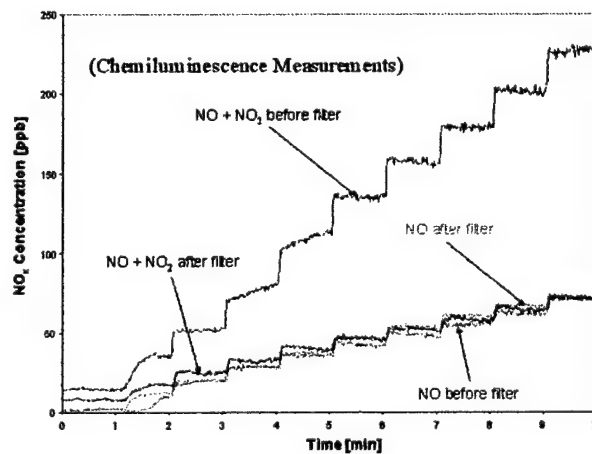


FIGURE 13 – Effect of silicalite molecular sieve filter on NO and NO_2 concentrations before and after the filter.

Results shown in Figure 13 illustrate the ability of the silicalite filter to remove NO_2 while leaving the NO concentration unchanged. The chemiluminescence monitor was used to quantify the concentration of NO and NO_2 before and after the filter. The concentration of a mixture of NO and NO_2 in air was increased in 1 minute intervals. The NO concentration before the filter and after the filter is shown to be similar within about 10%, which is the limitation of the reproducibility of the delivery system. By using a converter to reduce NO_2 to NO , the additional NO generated provides a measure of the NO_2 originally present in the stream. The concentration of $\text{NO} + \text{NO}_2$ before the filter shows that the initial mixture contains approximately 2/3 NO_2 and that the amount of NO_2 remaining after the filter is below detection limits. Thus, we conclude that the silicalite removes the NO_2 completely while allowing the NO to pass unattenuated.

Having filtered organic compounds and NO_2 from the breath sample, and shown that the sensor responds to NO_2 but not to NO , we now discuss the possibilities for conversion of NO in an oxygen/nitrogen (air) ambient to NO_2 . Thermodynamically, the conversion of NO to NO_2 is favorable; however, the change in free energy for the reaction is only -8.45 kcal/mol at 298 K (the equilibrium constant, $K = 1.4 \times 10^6$) but becomes less favorable at higher temperatures. We should note that, although the free energy of formation for NO and NO_2 are positive, $\Delta G_f(\text{NO}) = 20.697 \text{ kcal/mole}$ and $\Delta G_f(\text{NO}_2) = 12.247 \text{ kcal/mol}$, the equilibrium concentration of NO_2 in a mixture of N_2 and O_2 is of order 1 ppb. A catalyst which can activate the reaction of NO with O_2 in the breath sample is not limited thermodynamically in the conversion to NO_2 for quantitative purposes. However, if the catalyst can activate N_2 as well as O_2 , then NO_2 production from N_2 and O_2 in the breath stream may be expected at the 1ppb level, leading to a potential background source of NO_2 .

The reaction of NO with permanganate has the advantage of avoiding the oxidation of nitrogen in the breath sample, but the disadvantage that it is a consumable item which must be replenished periodically. The results shown in Figure 14 reveal that NO can be converted to NO_2 over an

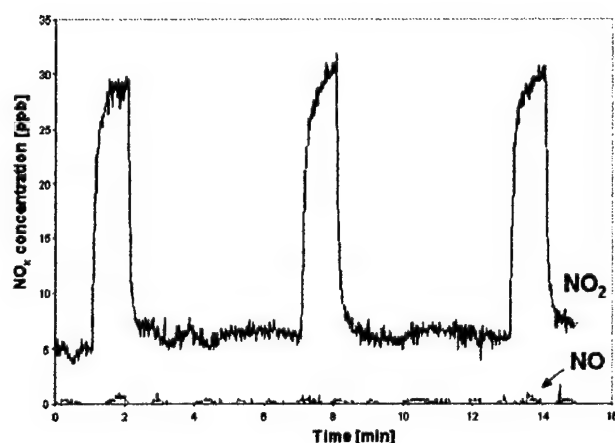


FIGURE 14 – Oxidation of NO to NO_2 with $\text{KMn}_4/\text{Al}_2\text{O}_3$. Concentration of NO and NO_2 produced following three pulses of air containing 60 ppb NO , as determined by chemiluminescence measurements.

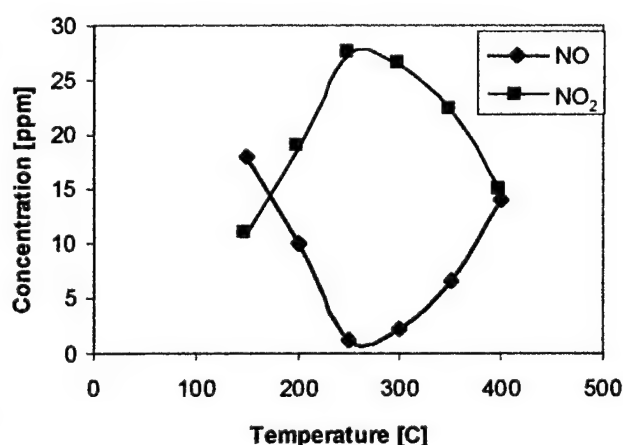


FIGURE 15 – Oxidation of NO to NO_2 with a platinum catalyst. Product distribution as a function of temperature with a feedstock containing 26.8 ppm NO and 2 ppm NO_2 in an air carrier gas.

alumina supported permanganate filter. The chemiluminescence monitor shows that air containing 60 ppb of NO is converted to NO₂ leaving negligible amounts of NO; however, the yield was about 40%, perhaps due to adsorption of NO₂ on the alumina support. The results in Figure 15 are for the conversion of NO in air over a platinum black catalyst (Alfa Aesar, 27 m²/g) contained in a quartz tube heated with nichrome wire. The results show that as the temperature increases, conversion improves to nearly 100% until at temperatures above 250°C, the conversion becomes limited thermodynamically. Thus, the catalyst provides a lower maintenance alternative to the permanganate oxidizing agent with higher conversion.

The results of the overall operation of the prototype system with human breath samples is demonstrated in Figure 16. The breath sample contains NO, a range of organic compounds which are potential interferences, and a high relative humidity. The humidity is first stabilized with minimal loss of NO, then filtered to remove non-polar compounds with one or more molecular sieves of appropriate pore size. The effluent contains NO, N₂, O₂, and H₂O, but may also contain H₂, CH₄, CO, and CO₂. The NO must then be oxidized to NO₂, since we find that the sensor response to NO is negligible compared to NO₂. Finally, the response of the SMO sensor is quantified and compared to calibration pulses of NO to determine the concentration in the breath sample. Test data were acquired from human breath samples using a standard addition method. The data points were taken from 7 separate experimental runs with 4 different people. The results shown in Figure 16A reveal a correlation between NO concentration and sensor response over the 0 - 100 ppb range, when using the permanganate oxidizing agent but not the silicalite filter. Note the low correlation coefficient of 0.75. Results with both the permanganate oxidizing agent and the silicalite filter, shown in Fig. 16B, are much improved. The correlation between the sensor response and the actual NO concentration, as determined by the chemiluminescence monitor, fits a linear dependence as shown with a correlation coefficient of 0.96. The negative intercept may reflect incomplete removal of isoprene by the filter as well as other larger hydrocarbons which are too large to be absorbed in the pore structure of the silicalite. However, the reproducibility is on the order of several ppb which is adequately sufficient for use in a practical device.

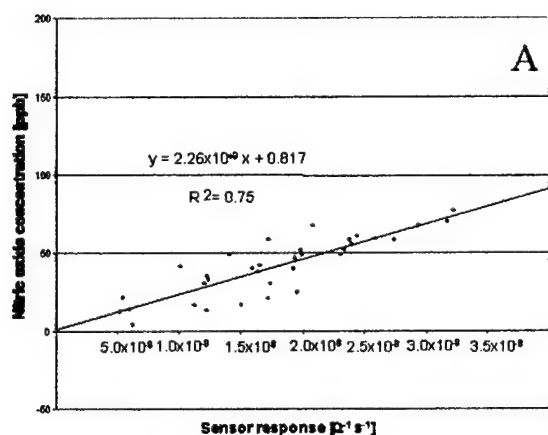


FIGURE 16A – Sensor response to NO in human breath using the KMn₄/Al₂O₃ oxidizing agent without the silicalite filter.

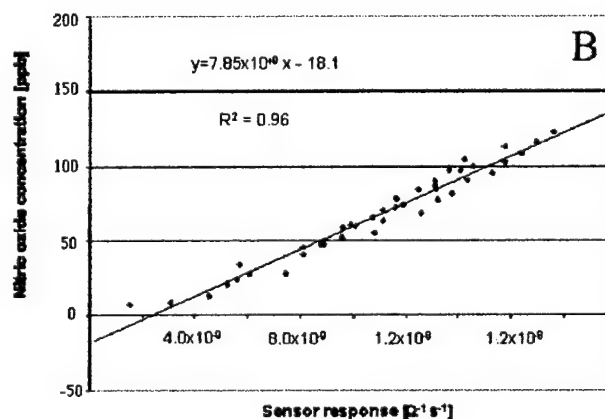


FIGURE 16B – Sensor response to NO in human breath using the KMn₄/Al₂O₃ oxidizing agent and the silicalite filter. Note the improvement in the correlation coefficient.

A photograph of the prototype NO detection system is shown in Figure 17. The SMO sensing element is very compact as shown on the figure. The electronic components could easily be miniaturized in a next generation prototype.

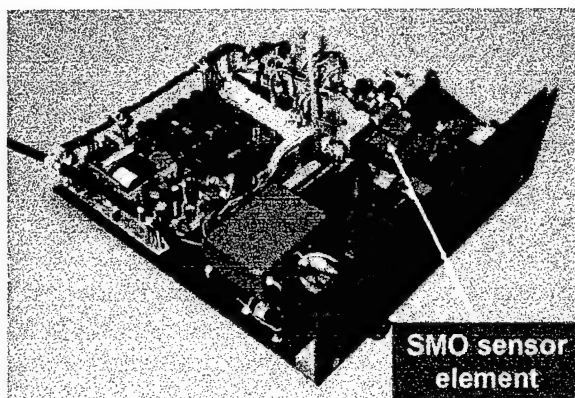


FIGURE 17 – Photograph of the prototype NO monitor system.

6. Mass Spectral Measurements of Other Biomarkers in Human Breath

Under Option II funding of the grant, the research program was expanded to include investigations of other various components of human exhaled breath as potential markers of health and disease. The goal of this work was to determine whether analysis of these other components are complementary to NO diagnostics. The experiments were performed using a Fourier transform ion cyclotron resonance (FT-ICR) mass spectrometer that acquires ultra-high resolution mass spectra. The FT-ICR is equipped with the external and internal electron impact ionization and it is possible to perform chemical ionization as well; the CI 'soft ionization' can be used to reduce ion fragmentation. The electron impact ionization sources and the vacuum chamber were installed and accurate calibration procedures were developed with the new instrument. A database of several calibration gases (e.g., cyclopropane, ethanol, acetone, pentane, isoprene) that were presumed to be present in real breath samples was established for comparison with actual samples. The advantage of FT-ICR MS is that ultra-high resolution mass spectra with high mass accuracy (~ 1 ppm) can be acquired, and unknown analytes can be identified based on mass measurement accuracy alone.

We designed, constructed and examined four different instrumental configurations to identify various analytes that are present in human exhaled breath. A 7 tesla IonSpec (Irvine, CA) Fourier transform ion cyclotron resonance (FT-ICR) mass spectrometer interfaced to an SRI 8610C GC (Las Vegas, NV) and/or a model 7100 Entech preconcentrator (Simi Valley, CA) was utilized to perform mass spectral analyses. Initially, the commercial mass spectrometer was added to an existing actively shielded 7 tesla superconducting magnet. The stray field of the shielded magnet drops off rapidly (< 50 gauss at a distance of ~ 1 meter) and this allows for convenient addition of other components to the mass spectrometer. The mass spectrometer was purchased, installed and calibrated using various analytes. Subsequently, an SRI 8610C GC (Las Vegas, NV) and a model 7100 Entech preconcentrator (Simi Valley, CA) were interfaced to the FT-ICR and experiments were performed. In-house instrumental modifications were made to the gas chromatographic interface and mass spectrometer as needed. The instrument can be used in

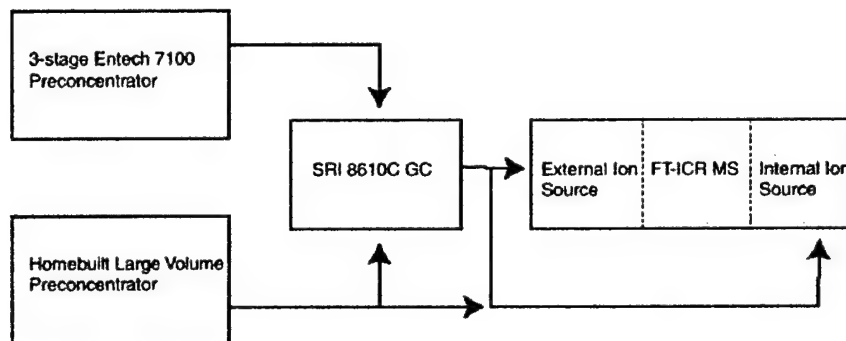


FIGURE 18 – Configuration of the FT-ICR mass spectrometer system.

either a) Direct MS mode, b) External GC MS mode, c) Internal GC MS mode, and d) Preconcentrator coupled to “b” or “c” mode. Figure 18 shows a schematic of the various mass spectral analysis modes. The 7100 preconcentrator is designed to perform gas-phase analyte preconcentration using up to three trapping stages. Figure 19 shows the combined preconcentration, sampling, and data analysis schemes.

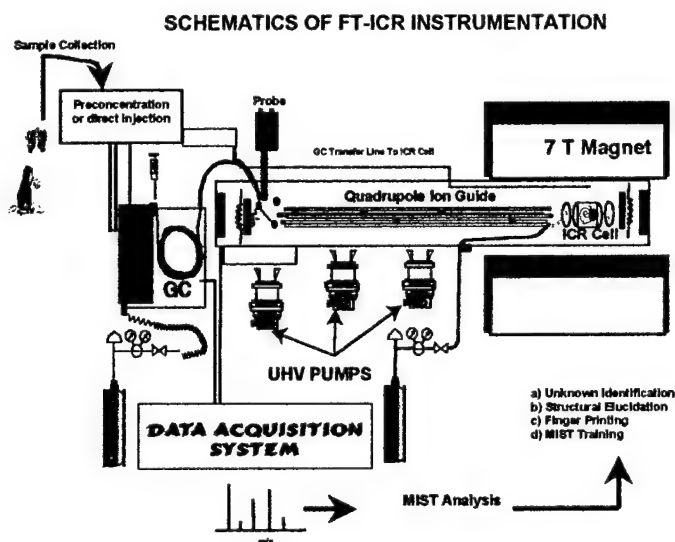


FIGURE 19 – Major components of the combined preconcentrator, gas chromatograph, FT-ICR instrument.

For GC experiments, samples were injected onto a 15m or 60m MXT Restek capillary column housed in a SRI (Las Vegas, NV) model 8610C GC. The effluent from the capillary column is directed into an SGE glass molecular jet separator. Both the GC column and molecular jet separator are located in the GC oven maintained at 70°C. The molecular jet separator reduces the helium flowing into the mass spectrometer (internal or external sources) by 99% and that of analyte about 70 to 90% depending on the analyte molecular weight. The remaining helium and analyte are transferred through a heated capillary line to the external or internal ion sources.

Figure 20 shows a typical sequence of events for the GC FT-ICR experiment. Sample is first injected into the GC and analytes elute from the column at different retention times. Once the analyte molecules elute from the GC transfer line into the mass spectrometer ion source, electron

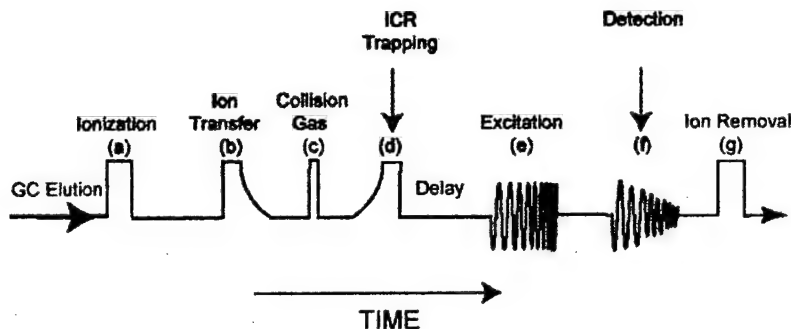


FIGURE 20 – Event sequence for a typical GC FT-ICR experiment.

impact or chemical ionization occurs (Figure 20a). Analyte ions are transferred into the ICR cell (Figure 20b) and a short pulse (3-20 ms) of N_2 gas is introduced to increase the ICR cell pressure (up to $\sim 1 \times 10^{-6}$ torr) and to cool ion axial motion (Figure 20c). Appropriate timing and/or gated trapping techniques are used to trap the ions inside the ICR cell (Figure 20d), a variable delay period (100 ms- 50 s) is used for partial restoration of the base pressure. Charge transfer inside the ICR cell is reduced at shorter delay times (< 1 s) and hence mass spectra resemble normal EI spectra. At longer delay times (> 1 s), a sufficient number of collisions can occur and ion abundance of the analytes with higher proton affinity may increase; this is an excellent alternative to increase selective sensitivity. The limitation for having longer reaction delay time in GC FT-ICR experiments is that a sufficiently high duty cycle rate is needed to adequately define the GC peaks; in practice, optimization is performed experimentally and parameters may depend on the analyte and the class of compounds. The trapped ions are excited (Figure 20e) by a dipolar frequency sweep excitation and detected in the direct broadband mode (Figure 20f). In order to prepare the system for the next experimental event sequence, at the end of each experiment, all trapped ions are ejected from the ICR cell (Figure 20g). Mass spectra were constructed either from a single time-domain data set or averaged time-domain signals (normally 128 or 256 kiloword data points per time-domain transient signal). The FT-ICR mass spectra are obtained through Fourier transformation of the resulting time-domain signal with one zero-fill, baseline correction and Hamming apodization followed by magnitude calculation and frequency-to-mass conversion.

Figure 21 shows a representative EI FT-ICR mass spectrum from direct analysis of human exhaled breath. The inset on the left shows the time-domain transient signal before Fourier transformation. As expected, the most abundant species in human exhaled breath include water, nitrogen, oxygen and carbon dioxide. The inset on the right panel shows an expanded view of the $m/z = 29.9$ region. Note that the low-abundance nitrogen oxide peak can be observed in the presence of very abundant major peaks such as nitrogen and oxygen. The excellent agreement between theoretically calculated (T) and experimentally determined (E) mass-to-charge ratios for the NO demonstrates the mass measurement accuracy of FT-ICR mass spectrometry.

Rapid identification of the unknown analytes requires several steps and we have written a computer program, Mass Identification Smart Tool (MIST) to perform this task. In order to assign the true identify of unknown analytes, it is critical to calibrate the acquired mass spectra to within a few parts per million (ppm) mass measurement accuracy. MIST is a software tool that

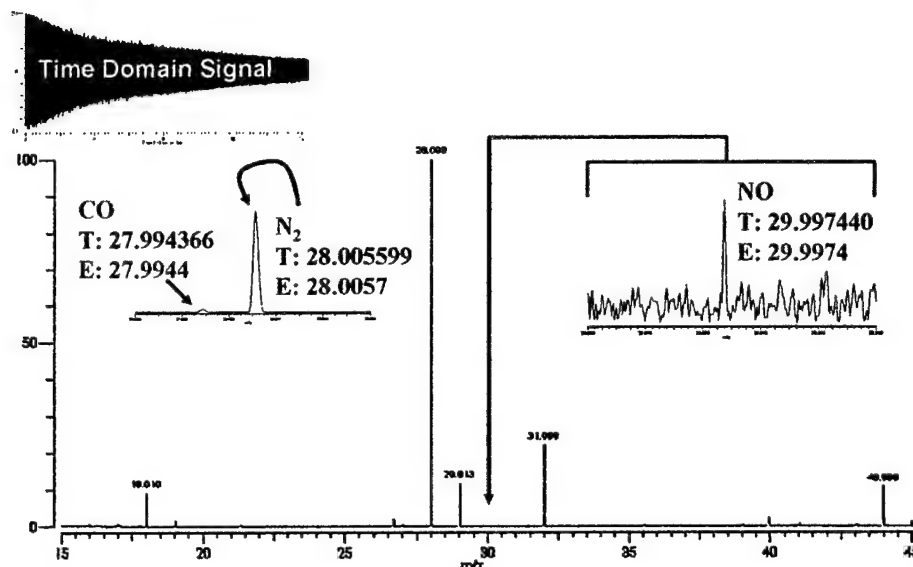


FIGURE 21 – Direct 70 eV EI FT-ICR mass spectrum from human exhaled breath.

we have written to search for combinations of atomic masses that add up to a mass value set by a user (input from FT-ICR data). The accuracy of the search in ppm and the extent of the search in terms of number and type of elements to search for, are set by the user (input from the FT-ICR calibration table and a knowledge about the unknown analyte class). With the available input information the program creates a two-dimensional array or table of all possible mass combinations. The table is composed of identical columns each containing a sorted one-dimensional array of possible masses. The search process involves combining a mass value from one or more of these columns until all possible mass values (output) that equal the desired input m/z value within the specified accuracy (input in ppm) are found and printed on the computer screen. To improve accuracy, the program automatically adds or subtracts the mass of an electron from the total mass to charge values for negative and positive ion searches, respectively. The program uses a binary search and a rule guided walking technique to minimize the search time through the table. Users can teach MIST how likely specific combinations of atoms might occur in nature so that MIST can further filter and refine future searches.

Summary of the required steps for unknown identification is shown in Figure 22 for a human breath sample. First ultra-high resolution FT ICR mass spectra are acquired and mass calibrated with internal or external calibrants. Based on the exact mass measurement alone various unknown analytes are identified. Once the mass spectrum is calibrated, the mass calibrated values are subjected to Mass Identification Smart Tool (MIST) analysis.

Figure 23 shows a representative FT-ICR mass spectrum including expanded m/z regions from analysis of the human exhaled breath in direct pulsed FT-ICR mode. The breath was collected for 10 minutes in a coiled copper tube sample reservoir immersed in a dry ice bath. The sample reservoir was allowed to warm to room temperature before installation on the pulsed collision gas reservoir port of the FT-ICR MS. The pulsed collision gas reservoir and its line to the sample reservoir were evacuated. The headspace in the sample reservoir was transferred to the pulsed gas collision gas reservoir to an indicated pressure of 50 torr. After a few minutes, the HEB

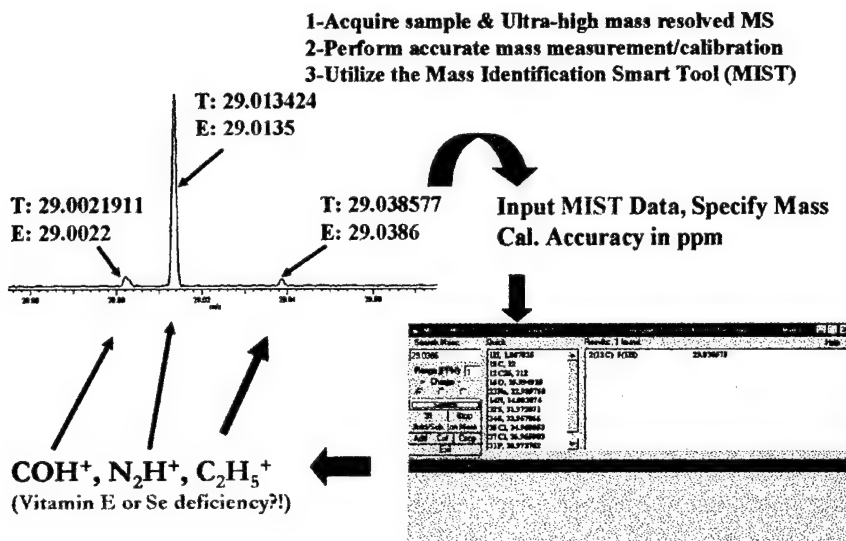


FIGURE 22 – Steps required to identify unknown analytes in human breath using MIST software.

sample in the collision gas reservoir was pulsed (for 3 ms) into the FT-ICR MS analyzer region for mass spectral analysis. The positive ion mass spectrum was acquired circa 20 s after a 200ms pulse of 70 eV electrons had been admitted into the analyzer cell to effect ionization. The m/z 15 to 100 region clearly shows the major components: water (as protonated water) at m/z 19.018 and oxygen at m/z 31.989. The reaction time inside the ICR cell was sufficiently long for complete removal of [N₂]⁺ species via charge transfer processes such as to water and oxygen.

An expanded view of the m/z 40 to 70 Th region shows several peaks, and their assignments from accurate mass measurement analysis are as follows:

Exp. Mass	Accurate Mass	Assignment
43.017	43.017	C ₂ H ₃ O ⁺ acetyl cation, an EI fragment from acetone
45.033	45.033	C ₂ H ₅ O ⁺ an EI fragment from ethanol
47.048	47.049	C ₂ H ₇ O ⁺ protonated ethanol
57.069	57.070	C ₄ H ₉ ⁺ t-butyl cation
58.040	58.040	C ₃ H ₆ O ⁺ acetone molecular cation
59.048	59.049	C ₃ H ₇ O ⁺ protonated acetone
60.020	60.021	C ₂ H ₄ O ⁺ methyl formate or acetic acid molecular ion
61.027	61.028	C ₂ H ₅ O ₂ ⁺ protonated acetic acid or methyl formate
69.067	69.070	C ₅ H ₉ ⁺ protonated isoprene

The expanded view of the m/z 42.8 to 47.2 Th region clearly shows that the peak at a nominal m/z 47 Th is a doublet. The peak assignments for these species are:

47.012	47.013	CH ₃ O ₂ ⁺ protonated formic acid
47.048	47.049	C ₂ H ₇ O ⁺ protonated ethanol

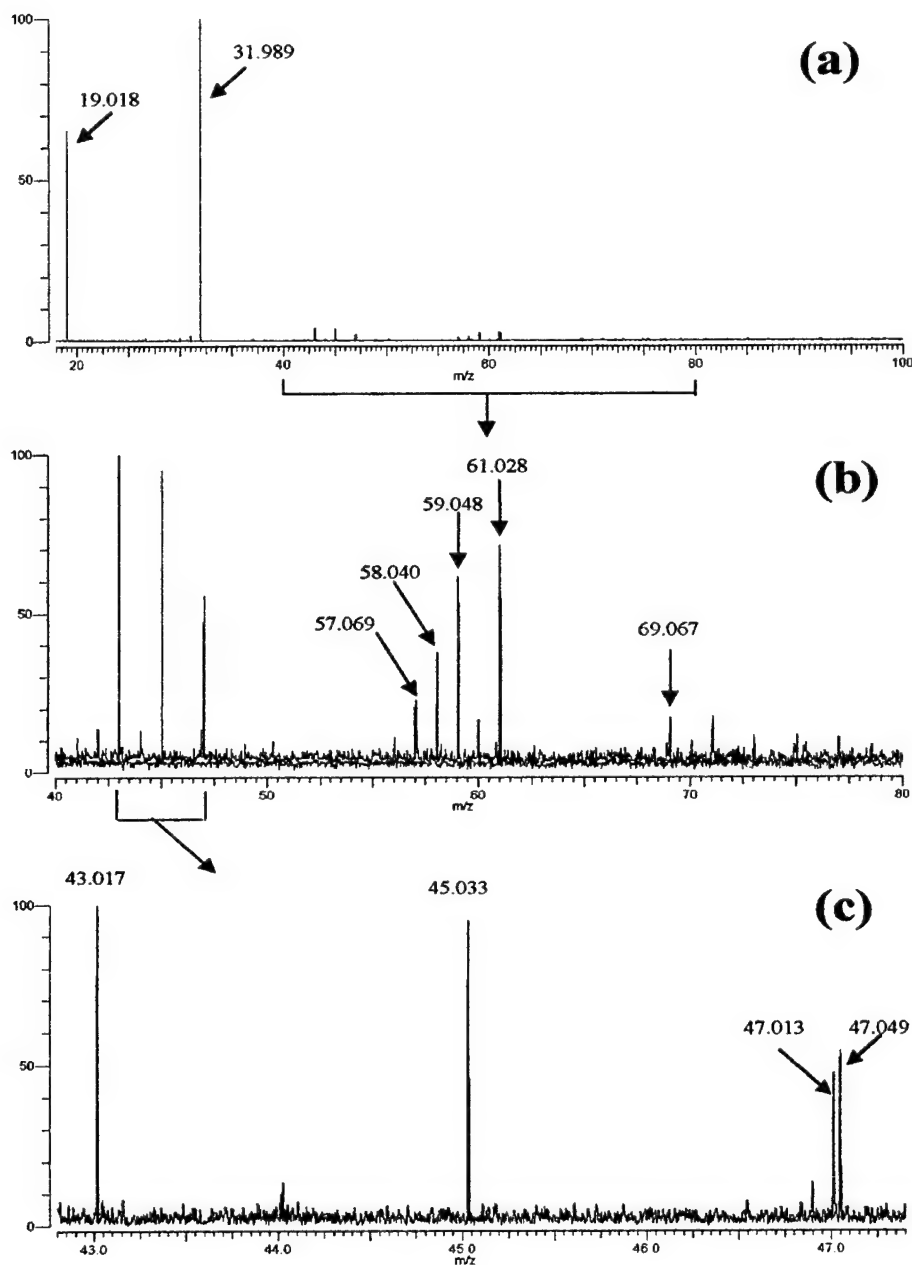


FIGURE 23 – Positive ion direct pulsed mode FT-ICR mass spectrum from a preconcentrated sample of "healthy" human breath.

A list of identified components that are present in exhaled breath of the subjects we tested is given in Table II. Excluding the major inorganic components such as N_2 , CO_2 , O_2 , H_2O , etc., acetone and ethanol are the organic compounds that are present in the "healthy" male HEB at the highest concentrations. Relative abundance of ethanol is always higher than the acetone and our results indicate that the ratio of [ethanol]/[acetone] may vary from one individual to the next. A more quantitative comparison will require additional and better-calibrated external ions source data. Protonated methyl formate or acetic acid (m/z 61.0284 Th and 61.0396 Th, respectively) as well as methanol and isoprene are also minor components that are at higher concentration than other organic molecules.

TABLE II. Library of Various Components in "healthy" human exhaled breath.

<u>Accurate Mass</u>	<u>Assignment</u>	<u>Mol. Form.</u>
15.9944	EI Fragment Ion	O^+
18.0100	Water	H_2O^+
19.0178	Protonated Water	H_3O^+
27.9944	Carbon Monoxide	CO^+
28.0056	Nitrogen	N_2^+
28.0308	Ethylene	$C_2H_4^+$
29.0022	Protonated Carbon Monoxide	HCO^+
29.0134	Protonated Nitrogen	HN_2^+
29.0386	Ethyl Cation	$C_2H_5^+$
29.9974	Nitric Oxide	NO^+
31.0178	Methanol $[M-H]^+$	CH_3O^+
31.9893	Molecular Oxygen	O_2^+
32.0257	Methanol	CH_4O^+
35.9761	Hydrogen Chloride	HCl^+
43.0178	Acetyl (acetone EI fragment ion)	$C_2H_3O^+$
43.0542	Propyl Cation	$C_3H_7^+$
43.9893	Carbon Dioxide	CO_2^+
44.9971	Protonated Carbon Dioxide	CHO_2^+
45.0335	Ethanol $[M-H]^+$ (ethanol EI fragment ion)	$C_2H_5O^+$
47.0128	Protonated Formic Acid	$CH_3O_2^+$
47.0491	Protonated Ethanol	$C_2H_7O^+$
57.0335	Acetone $[M-H]^+$ (acetone EI fragment ion)	$C_3H_5O^+$
57.0699	t-Butyl Cation?	$C_4H_9^+$
58.0413	Acetone	$C_3H_6O^+$
59.0491	Protonated Acetone	$C_3H_7O^+$
61.0284	Protonated Methyl Formate or Acetic Acid	$C_2H_5O_2^+$
61.0396	Protonated Urea	$CH_5N_2O^+$
61.0648	Protonated Propanol	$C_3H_9O^+$
69.0699	Protonated Isoprene	$C_5H_9^+$
71.0855	HC	$C_5H_{11}^+$
73.0284	?	$C_3H_5O_2^+$
73.0648	Protonated Butanone	$C_4H_9O^+$
75.9436	Carbon Disulfide	CS_2^+
79.0542	Protonated Benzene	$C_6H_7^+$
85.1012	HC	$C_6H_{13}^+$
91.0542	HC	$C_7H_7^+$
105.0335	?	$C_7H_5O^+$

Figure 24 compares results acquired from breath samples for a non-smoker versus a smoker test subject. Several additional species are present in the smoker's breath including benzene, furan, and toluene, indicating that the breath samples have significant "finger prints" that can be exploited for both routine analysis as well as for health diagnostics. Further work will continue in this area.

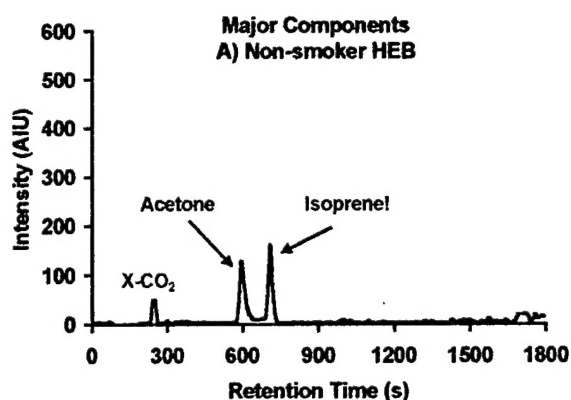


FIGURE 24A – FT-ICR spectrum from a healthy non-smoker test subject.

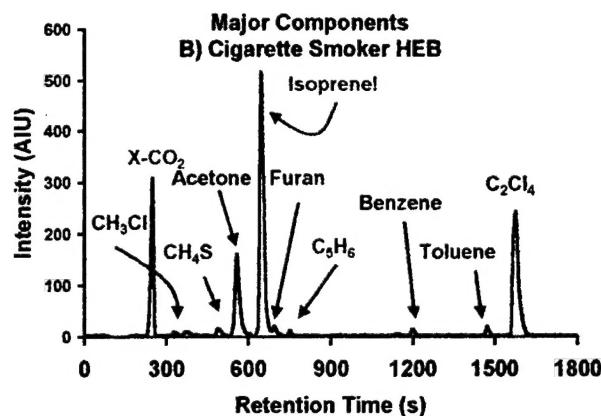


FIGURE 24B – FT-ICR spectrum from a healthy smoker showing additional exhaled species.

7. Research Publications and Presentations - Grant # N65236-998-1-5415

"Detection and Quantification of Nitric Oxide in Human Breath using a Semiconducting Metal Oxide Based Chemiresistive Microsensor," B. Fruhberger, N. Stirling, F. G. Grillo, S. Ma, D. Ruthven, R.J. Lad, B. G. Frederick, 8th International Meeting on Chemical Sensors, Basel, Switzerland, 3-5 July (2000).

"Detection and Quantification of Nitric Oxide in Human Breath using a Semiconducting Metal Oxide Based Chemiresistive Microsensor," B. Fruhberger, N. Stirling, F.G. Grillo, S. Ma, D. Ruthven, R.J. Lad, B.G. Frederick, *Sensors and Actuators B* **76**, 226 (2001).

"Heteroepitaxial Growth of Tungsten Oxide Films on Sapphire for Chemical Gas Sensors," S.C. Moulzolf, L.J. LeGore, and R.J. Lad, *Thin Solid Films* **400**, 56 (2001).

"Stoichiometry and Microstructure Effects on Tungsten Oxide Chemiresistive Films," S.C. Moulzolf, S.A. Ding, and R.J. Lad, *Sensors and Actuators B* **77**, 375 (2001).

"Performance of Zr and Ti Adhesion Layers for Bonding of Platinum Metallization to Sapphire Substrates," G. Bernhardt, S. Silvestre, N. LeCursi, S.C. Moulzolf, D.J. Frankel, and R.J. Lad, *Sensors and Actuators B* **77**, 368 (2001).

"Waiting to Exhale: Meeting News from the Federation of Analytical Chemistry & Spectroscopy Societies (FACSS)" PC GC FT-ICR for Exhaled Breath Analysis," Harris, C. M. (discussion of significant research by T. Solouki, J. Szulejko, B. Frederick, R. Lad), *Anal. Chem.* **73**, 658A-659A (2001).

"Using External and Internal Calibrants to Identify Pyrolysis Products of Suwannee River Fulvic Acids," Paul Kutia, Touradj Solouki, University of Maine Honors Undergraduate Thesis (2001).

"Coupling a Gas Chromatograph to a Fourier Transform Ion Cyclotron Resonance Mass Spectrometer: Biological and Environmental Mass Spectrometry," Touradj Solouki, Jan E. Szulejko, 49th ASMS Conference on Mass Spectrometry and Allied Topics, American Society for Mass Spectrometry, Chicago, IL, WPM 266 (2001).

"The Use of Ultra-high Resolution Fourier Transform Ion Cyclotron Resonance Mass Spectrometry for Rapid Detection and Identification of Various Species in Human Exhaled-Breath: Disease Diagnosis," Jan E. Szulejko, David Labrecque, Touradj Solouki, 49th ASMS Conference on Mass Spectrometry and Allied Topics, American Society for Mass Spectrometry, Chicago, IL, WPQ 331 (2001).

"Gas Chromatography And Fourier Transform Ion Cyclotron Resonance Mass Spectrometry: Analyzing Complex Sample Mixtures," Touradj Solouki and Jan Szulejko, NERM 2001 Invited Symposium: Oral Platform, Developments In Mass Spectrometry B. Instrumentation, Durham, NH, June 24-27 (2001).

"Fingerprinting Complex Biological and Environmental Samples: Biomarkers Identification with A High Performance Mass Spectrometer," Touradj Solouki, Invited Symposium, "New Investigators In Analytical Science: Innovative Leaders In The New Millennium: 2001 FACSS Meeting, Detroit, MI (2001).

"Heteroepitaxy of Tungsten Oxide Films on Sapphire and Silicon for Chemiresistive Sensor Applications," R.J. Lad, IEEE Sensors Symp. Proc. 44.1 (2002).

"Identification of Surface Sites on Monoclinic WO₃ Powders by Infrared Spectroscopy," S. M. Kanan, Z. Lu, J. K. Cox, G. Bernhardt and C.P. Tripp, Langmuir 18, 1707 (2002).

"Synthesis of Nano-sized Monoclinic WO₃ Particles Using Chelating Ligands and Emulsion Based Methods," Z. Lu, S. M. Kanan and C.P. Tripp, Chemistry of Materials 12, 983 (2002).

"Breath Diagnostic Sensors as a Triage Tool for Pathogenic Exposure," B.G. Frederick, T. Solouki, R. Riker, R.J. Lad, AVS Topical Conference on Understanding and Operating in Threat Environments, Monterey, CA, May 1 (2002).

"Biomedical and Environmental Applications of a Preconcentrator Coupled to a Gas Chromatograph Fourier Transform Ion Cyclotron Resonance Mass Spectrometer" Touradj Solouki, Jan E. Szulejko, 50th ASMS Conference on Mass Spectrometry and Allied Topics, American Society for Mass Spectrometry (2002).

"High Resolution Biomarker Identification in Human Exhaled Breath of Smokers and Non-Smokers, and Cigarette Smoke: Connectivities to Chronic Obstructive Pulmonary Disease (COPD)," Jan E. Szulejko, Bob Walter, George O'Connor, Touradj Solouki, 50th ASMS Conference on Mass Spectrometry and Allied Topics, American Society for Mass Spectrometry (2002).

"Potential Analytical Applications of Interfacing a GC to an FT-ICR MS: Fingerprinting Complex Sample Matrices," Jan E. Szulejko and Touradj Solouki, Analytical Chemistry 74, 3434 (2002).

"Biomedical and Environmental Applications of a Preconcentrator Coupled to a High Performance Fourier Transform Mass Spectrometer for Characterization of Biota Matter Based on Their VOC Signatures: Arbor and Human Breathprinting," Jan E. Szulejko and Touradj Solouki, Analytical Chemistry, submitted (2002).

"Interfacing a GC to an FT-ICR-MS: Molecular Composition of Unknowns from Accurate Mass Measurement," Jan E. Szulejko and Touradj Solouki, Journal of American Chemical Society for Mass Spectrometry, submitted (2002).

"Using External and Internal Calibrants to Identify Pyrolysis Products of Suwannee River Fulvic Acids," Paul Kutia, Darren Heald and Touradj Solouki, Journal of Macromolecules, submitted (2002).